Pedestal structure and stability at low collisionality in TCV

L. Frassinetti[1], B. Labit[2], M. Dunne[3], A. Merle[2], H. Nyström[1], S. Saarelma[4], N. Vianello[5], the TCV Team[2].

[1]Division of Fusion Plasma Physics, KTH Royal Institute of Technology, Stockholm SE
[2]Ecole Polytechnique Fédérale de Lausanne (EPFL), Swiss Plasma Center (SPC), Lausanne, Switzerland
[3]Max-Planck-Institut für Plasma Physik, Boltzmannstr.2, 85748 Garching, Germany
[4]UKAEA Culham, Culham Science Centre, Abingdon, Oxfordshire, OX14 3DB, United Kingdom
[5]Consorzio RFX, Corso Stati Uniti 4, 35127 Padova, Italy

ITER will operate at low pedestal collisionality ($\nu^*_{ee}{}^{ped}$) and high normalized separatrix density (n_e^{sep}/n_e^{ped}). The ITER pedestal collisionality is supposed to be sufficiently low ($\nu^*_{ee}{}^{ped}$<0.1-0.2) that the pedestal will be limited by peeling instabilities, rather than ballooning instabilities. Most of the present days machines, in particular in Europe, tend to operate at high pedestal collisionality, with ELMs typically triggered by the balloning modes. While pedestal physics has been well studied at the ballooning boundary, so far information on the pedestal behaviour at the peeling boundary has been described only in DIII-D [1].

This work investigates the pedestal behaviour at low $\nu^*_{ee}{}^{ped}$ in TCV, with emphasis to the pedestal performance and stability. Four datasets are used, as shown in figure 1. One dataset with high $\nu^*_{ee}{}^{ped}$ obtained at 170kA/-1.4T/low-δ and P_{NBH}=1MW. Another dataset with medium/high $\nu^*_{ee}{}^{ped}$ obtained at 170kA/-1.4T/low-δ, 1.2MW NBH and 0.9MW X3 ECRH (blue squares). Finally, two datasets at low-δ and high-δ (red circles and yellow triangles) with low $\nu^*_{ee}{}^{ped}$ obtained at 155kA/-1.4T, 1.0MW NBH and 1.1MW X2 ECRH. As shown in figure 1, the low ν^* datasets reach a collisionality range comparable to that expected in ITER. Within each dataset, all engineering parameters are constant apart the gas rate (Γ_D) during the H-mode phase which has been changed from shot to shot to produce a variation in n_e^{sep} (Γ_D has been varied from zero up to a maximum value necessary to remain in Type I ELMy H-mode or to have a good ECRH absorption). Unfortunately, at low ν^* it was not possible to reach ITER-relevant n_e^{sep}/n_e^{ped}. The empty circles in figure 1 highlight two couples of shots at low ν^* (red and orange circles) and high ν^* (cyan and blue circles) with low and maximum gas rate.

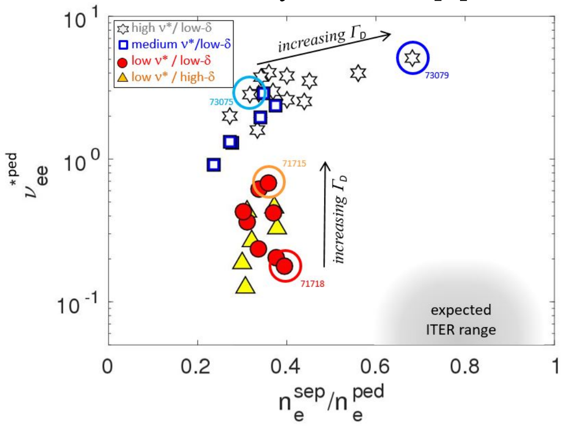

Figure 1. $\nu^*_{ee}{}^{ped}$ and n_e^{sep}/n_e^{ped} for the four datasets used in this work.

The electron pressure pedestal height (p_e^{ped}) is shown in figure 2. Figure 2(a) shows the correlation of p_e^{ped} with $\nu^*_{ee}{}^{ped}$ and figure 2(b) with electron density pedestal height (n_e^{ped}). At low collisionality ($\nu^*_{ee}{}^{ped}$<1), p_e^{ped} increases with increasing $\nu^*_{ee}{}^{ped}$ and with increasing n_e^{ped}. At high collisionality ($\nu^*_{ee}{}^{ped}$>1) the opposite trend is observed. The behaviour at high collisionality has been already reported in many machines [2,3,4] and it is due to the outwards shift of the density pedestal position (n_e^{pos}), driven by the increased gas rate, which shifts the pressure outwards and destabilizes the balloning modes. Instead, the behaviour at low ν^* was never observed before in a European machine, only DIII-D had so far observed a p_e^{ped} increase with increasing $\nu^*_{ee}{}^{ped}$ in type I ELMy H-modes. In the rest of the work we will investigate the causes of this behavior by analyzing the pedestal structure and stability.

The increase of p_e^{ped} in the low ν^* datasets is not due to the increase of the pedestal pressure gradient (∇p_e). As shown in figure 3(a), ∇p_e decreases with increasing n_e^{ped} both at low and high ν^*. Instead, the positive correlation between p_e^{ped} and n_e^{ped} at $\nu^*_{ee}{}^{ped}<1$ is due to the widening of the pedestal. As clearly shown in figure 3(b), at low ν^* the pedestal pressure width (w_{pe}) increases with increasing n_e^{ped}. At high collisionality, the width behavior is significantly different.

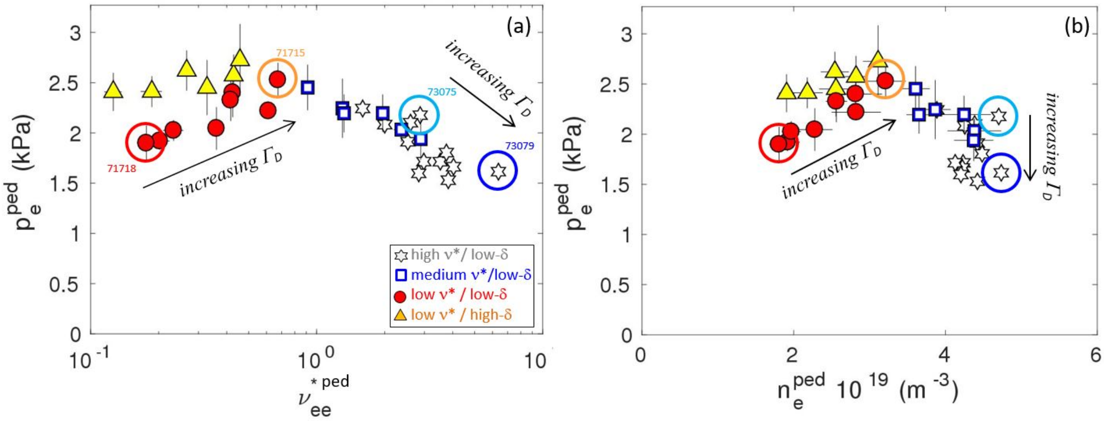

Figure 2. (a) p_e^{ped} versus $\nu^*_{ee}{}^{ped}$ and (b) p_e^{ped} versus n_e^{ped}.

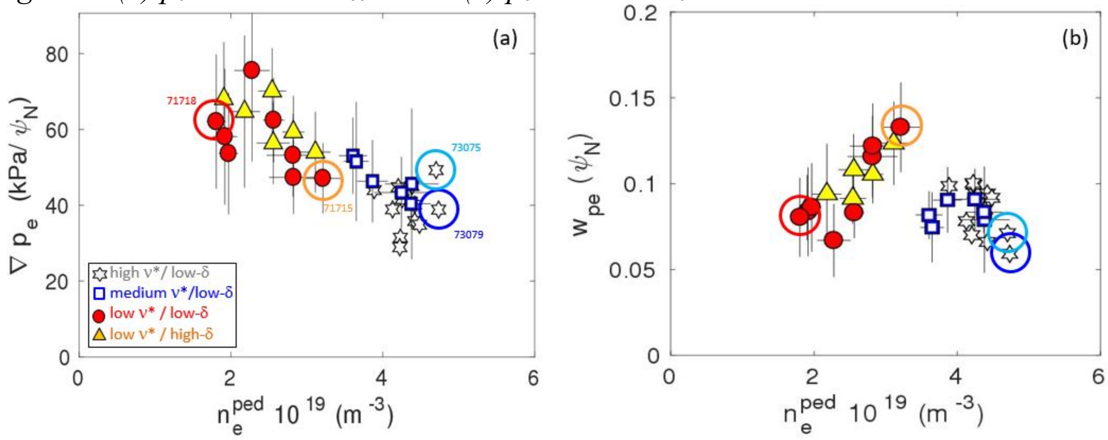

Figure 3. (a) maximum ∇p_e in the pedestal and (b) pressure pedestal width versus n_e^{ped}.

To understand the different pedestal behavior at low and high ν^*, the pedestal stability has been investigated. Figure 4 shows the peeling-ballooning (PB) stability diagram for the low $\nu^*_{ee}{}^{ped}$ pulse 71718 and for the high $\nu^*_{ee}{}^{ped}$ pulse 73079 done using KINX [5]. The low $\nu^*_{ee}{}^{ped}$ pedestal is near the nose of the PB stability, rather close to the peeling boundary, and limited by low-n modes (in the range n=5-10). Instead, the high $\nu^*_{ee}{}^{ped}$ pedestal isat the ballooning boundary, limited by high-n modes (n_{crit}=15-30). This suggests that the different pedestal behaviour at low and high collisionality is, at least in part, related to the different type of instabilities that trigger the ELMs.

To further investigate the link between experimental results and MHD stability, predictive pedestal modelling using the Europed code [6] has been done for the two low $\nu^*_{ee}{}^{ped}$ pulses and the two high $\nu^*_{ee}{}^{ped}$ pulses highlighted in figure 2. For each pulse, the predictions have been done for several values of the density. In each simulation, the density profiles has been rescaled and the ratio n_e^{sep}/n_e^{ped} has been kept constant. The results are shown in figure 5. Figure 5(a) shows the predicted p_e^{ped} vs n_e^{ped}. Some qualitative similarities between predicted and experimental results can be observed. First, at low ν^* the predicted p_e^{ped} tends to increase with increasing n_e^{ped}. The trend is however significantly weaker than experimentally observed (see figure 2). Second, at $n_e^{ped}\approx4\times10^{19}$ (m^{-3}) the predicted pressure has a sharp decrease with increasing n_e^{ped}. This transition is roughly consistent with the experimental results for which the different pedestal behaviour between low and high ν^* pedestals occurs at $n_e^{ped}\approx3.5\times10^{19}$

shown. n_{crit} is in the range 5-10 (consistent with peeling instabilities) at $n_e^{ped}<4\times10^{19}$ (m^{-3}) and in the range 50-70 (consistent with ballooning instabilities) at $n_e^{ped}>4\times10^{19}$ (m^{-3}). Note that the predictive modelling

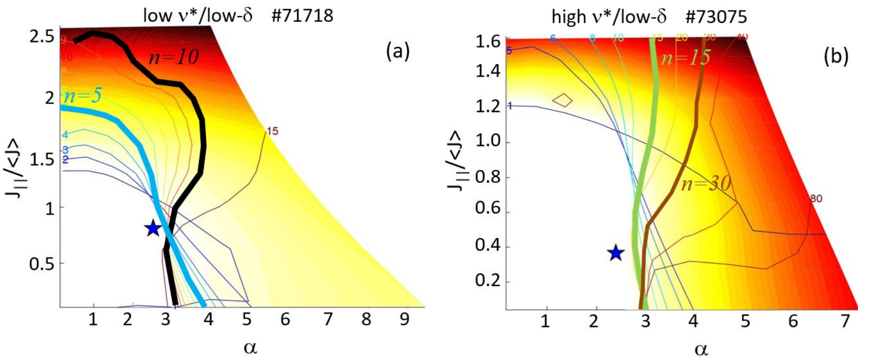

Figure 4. Peeling-ballooning stability diagram for the low $\nu^{*}_{ee}{}^{ped}$ pulse 71718 and for the high $\nu^{*}_{ee}{}^{ped}$ pulse 73075

(m^{-3}) as shown in figure 2(b). The transition in the predicted results is clearly due to the different type of instability, as shown in figure 5(b) where the most unstable mode vs n_e^{ped} is has a qualitative agreement with the experimental results also in terms of pressure gradient. The predicted normalized pressure gradient, α_{crit} in figure 5(d), has a negative correlation with n_e^{ped}, as also experimentally observed in figure 3(a).

We can highlight at least two clear differences between the predictions and the experimental results: (A) the behaviour of the pedestal width and (B) the behaviour of the two high ν^* pulses highlighted by the cyan and blue circles in figure 2(b).

(A) The behaviour of predicted and experimental width are significantly different at low ν^*, figures 5(c) and 3(b). Experimentally, the width increases with increasing n_e^{ped}, while the predictions show no clear increase. Instead, at high ν^* the width predictions are roughly in agreement with the experimental results ($w_{pe}\approx0.08\psi_N$) The predicted pedestal width has been determined using the KBM constraint which assumes turbulent transport driven by kinetic-ballooning microinstabilities. This suggests that the pedestal turbulent transport might be driven by different instabilities at low and high ν*. A preliminary experimental insight into the turbulent transport can be given via the η_e parameter, which is defined as $(\nabla T_e/T_e)/(\nabla n_e/n_e)$. As sown in figure 6(a), $\nabla n_e/n_e$ is clearly different between the low ν* datasets and the high ν* datasets. $\nabla T_e/T_e$ is also different between low and high ν* datasets, but in this case the transition from low to high ν* is smooth. Finally, η_e is clearly higher in the low ν* datasets, suggesting that the turbulent transport might be different from that in the high ν* datasets. This result is likely related to the different behaviour of the pedestal width, as higher transport can lead to wider w_{pe} [3].

(B) In the high ν* dataset, the increase of the

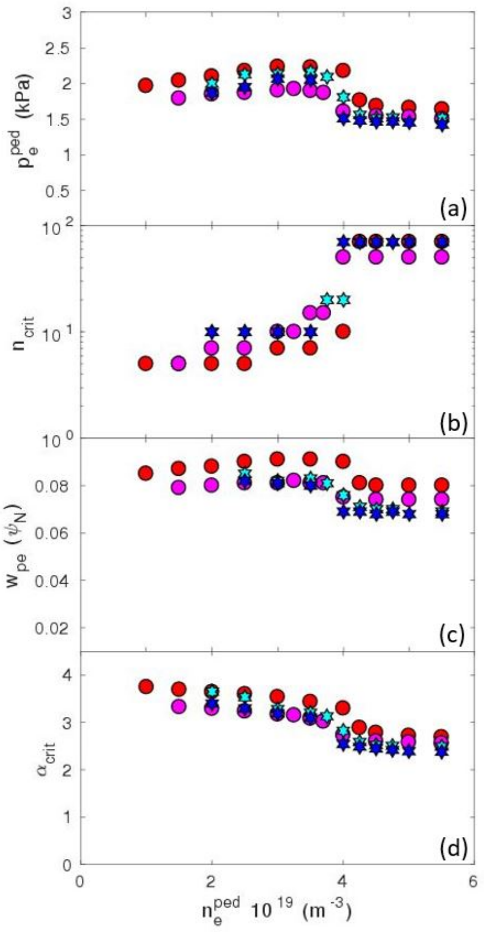

Figure 5. Europed predictive modelling for two low ν and two high ν* pedestals. (a) p_e^{ped}, (b) most unstable mode, (c) pressure width and (d) normalized pressure gradient versus n_e^{ped}.*

gas rate leads to a sharp reduction of p_e^{ped} (via T_e^{ped} reduction) but to no significant variation in n_e^{ped} (cyan and blue circle in figure 2).

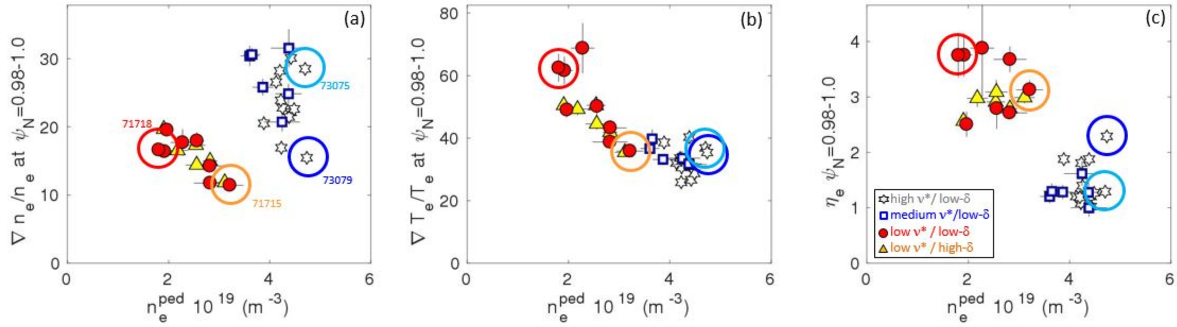

Figure 6. $\nabla n_e/n_e$ (a), $\nabla T_e/T_e$ (b) and η_e (c) averaged over ψ_N=0.98-1.00 versus n_e^{ped}

This behavior cannot be seen in the Europed scans of figure 5(a), where above $n_e^{ped}\approx 4\times 10^{19}$ (m^{-3}) the predicted p_e^{ped} is not significantly affected by n_e^{ped}. This is due to the fact that both n_e^{ped} and n_e^{sep} are input parameters in Europed and the scans in figure 5 are done assuming constant n_e^{sep}/n_e^{ped}. Interestingly, the behavior of n_e^{sep}/n_e^{ped} differs significantly between the low ν* and the high ν* datasets. This is shown in figure 7 where the pre-ELM density profiles for the pulses highlighted by circles in figure 2 are shown. At low ν*, the increase of the gas rate leads to the increase in both n_e^{ped} and n_e^{sep} with n_e^{sep}/n_e^{ped} remaining approximately constant (consistent with the modelling of figure 5). At high ν*, the increase of the gas rate leads to the increase in n_e^{sep} and in n_e^{sep}/n_e^{ped}, effectively shifting the density profiles outwards. As discussed in several earlier works [2,3,4], this destabilizes the balloning modes, decreases the pedestal stability and leads to lower p_e^{ped}. Obviously, this effect cannot be predicted by figure 5 as constant n_e^{sep}/n_e^{ped} has been assumed.

In conclusion, this work shows that at low collisionality ($\nu^*_{ee}{}^{ped}<1$) the pedestal pressure increases with increasing gas rate, a behaviour opposite to what observed at high ν*. This is linked to at least two reasons. First, n_e^{sep}/n_e^{ped} is approximately constant at low ν* (so the destabilizing effect of the increasing n_e^{sep}/n_e^{ped} is not present). Second, the pedestal is limited by low-*n* instabilities. Predictive modelling has some similarities with the experimental result (a sharp p_e^{ped} reduction at $n_e^{ped}\approx 4\times 10^{19}$ (m^{-3})) but also clear differences (no w_{pe} widening is predicted at low ν*). This might be due to a different turbulent transport which suggests that a more advanced transport constraint needs to be included in Europed. Finally, the different behaviour of the density at low and high ν* further strengthen the fact that fully reliable pedestal predictions can be achieved only if coupled with density predictions.

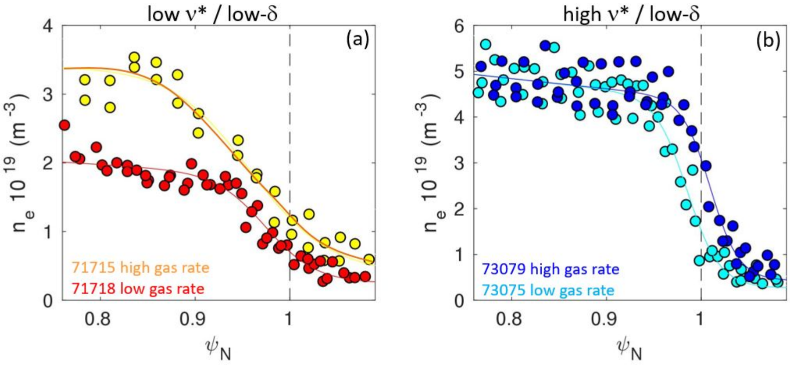

Figure 7. Electron pedestal pressure versus density for a low ν pulse (red square) and corresponding Europed modelling (blue) and most unstable modes.*

This work has been carried out within the framework of the EUROfusion Consortium, funded by the European Union via the Euratom Research and Training Programme (Grant Agreement No 101052200 — EUROfusion). Views and opinions expressed are however those of the author(s) only and do not necessarily reflect those of the European Union or the European Commission. Neither the European Union nor the European Commission can be held responsible for them.

REFERENCES

[1] Snyder P. et al., Nucl. Fusion 55, 083026 (2015)
[2] Dunne PPCF 2017
[3] Sheikh PPCF 2019
[4] Frassinetti NF2019
[5] Degtyarev L et al 1997 CPC 103 10–27
[6] Saarelma S et al., PoP 26, 072501 (2019)